ICANS XIX,
19th meeting on Collaboration of Advanced Neutron Sources
March 8 – 12, 2010
Grindelwald, Switzerland

Installation and Initial Operation of an On-Line Target Imaging System for SNS*

T. J. Shea

Oak Ridge National Laboratory (ORNL)
Oak Ridge, TN 37831, USA

and

T. McManamy[1], G. Bancke[2], W. Blokland[1], A. Brunson[3], M. Dayton[1], K. C. Goetz[4], J. Janney[1], M. Lance[1], C. Maxey[1], F. Montgomery[1], P. Rosenblad[1], S. Sampath[2], M. Simpson[1]

1. Oak Ridge National Laboratory (ORNL), 2. SUNY Stony Brook, 3. Caltech, 4. Dartmouth College

ABSTRACT

After several years of operation, the SNS now enters an era of megawatt class operation. At this intensity level, the target will be operating closer to its engineering limits and the beam profile on target must be carefully controlled. During commissioning and early operations, a temporary imaging system was used to measure the proton density on target. This system was not designed to survive the increasing power levels and it had to be removed in the second half of 2006. Since then, no direct measurement of beam properties at the target has been available. A collaboration was forged to remedy this situation, and has resulted in a new imaging system consisting of three major components: a thermal-sprayed luminescent coating deposited on the target nose, a radiation-tolerant optical system installed upstream of the target, and an image acquisition system integrated with the accelerator controls network. The design, installation, and integration of these components will be described. Initial beam measurements and image analysis results will be presented. Lessons learned during this initial operating experience have been documented and will guide the collaboration's future plans.

1. Motivation and Background

In operation since 2006, the Spallation Neutron Source at Oak Ridge National Laboratory now operates with approximately one megawatt of beam power on the Mercury target. This average power level is achieved with a 60 Hz pulse repetition rate, nearly 1 GeV beam energy, and single pulse intensity approaching 10^{14} protons per pulse. With a pulse length of less than 1 microsecond, cavitation can cause erosion of the stainless steel target wall. Inspection of the first target, replaced in the Summer of 2009, revealed this type of damage [1]. Since the damage rate is very sensitive to the peak beam power and transverse profile, direct monitoring of the beam properties at the target can help to assure maximum target lifetime. Based on the success of a temporary imaging system used only during the 2006 commissioning runs, an on-line system capable of withstanding full beam power was developed [2].

* Work supported by the US Department of Energy

2. System Development and Installation

2.1. Physical Layout

The new Target Imaging System (TIS) consists of three major subsystems: 1) a luminescent coating on the stainless steel water shroud of the target, 2) a radiation-tolerant optical system mounted to the proton beam window assembly, and 3) a camera and image acquisition system integrated with the accelerator control system. The locations of the coated target and the optical components are depicted in Fig. 1. During operation, the flight path between the parabolic mirror and the target is filled with Helium at atmospheric pressure. The fiber optic imaging cable is routed to an area that is accessible during full power operation. This allows hands-on maintenance of the image acquisition system, and also allows experiments involving manual setup. Plans for this system have been previously presented, so the following discussion is restricted to an overview, updated with experience from the recent installation [3].

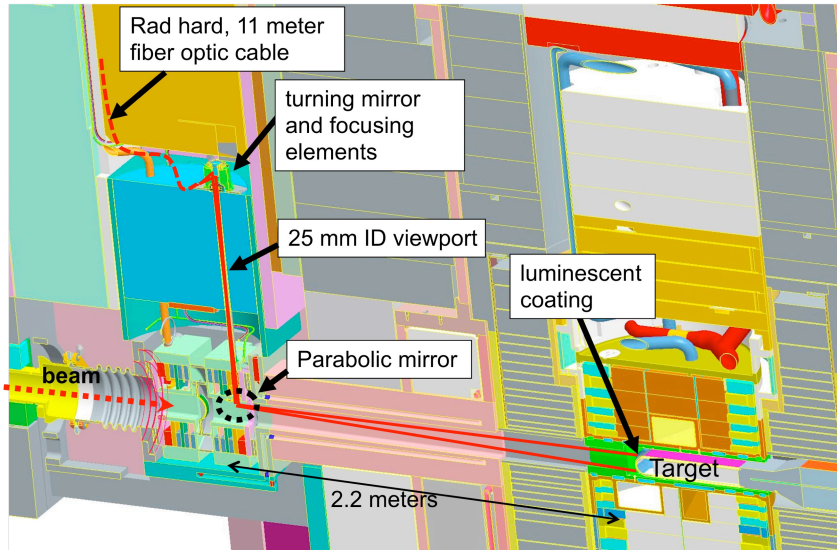

Fig. 1. Layout of the target imaging system.

2.2. Luminescent Coating

In many particle beam imaging applications, a freestanding luminescent screen intercepts the beam. Although this arrangement worked for the temporary system when average beam power did not exceed 10 kW, at high power the screen would exhibit temperature dependent efficiency and could eventually be destroyed. Bonding the luminescent material to the cooled target surface mitigates these issues and also avoids the mechanical complexities of other options.

Coating development proceeded for over one year and involved an extensive collaboration between multiple ORNL divisions and the Center for Thermal Spray Research at SUNY-Stony Brook. In applications with similar particle beams, Chromium doped alumina has demonstrated a long lifetime and was therefore the primary candidate for coating material. A combustion flame spray process was selected and optimized to achieve high luminescent efficiency, low substrate temperature, and adequate mechanical properties. Spray process variables included: powder composition and grain size distribution, spray distance, and gas and fuel flow rates. The resulting samples were tested

with X-ray diffraction to measure retention of the desired alpha phase, electron microscopy to observe the coating structure and chromium distribution, photo-stimulated luminescence to compare efficiency to that of standard sintered screens, and proton beam irradiation to simulate the final application. A typical spectrum from photo stimulation (with a green laser) is shown on the left in Fig 2. The two characteristic R-lines of Ruby are visible in sintered screen (higher amplitude) and the coating (lower amplitude). A beam spot from a ~ 1GeV proton test beam is visible on a coating sample on the right side of Fig. 2. The final coating achieved efficiency near 60% of the sintered screen.

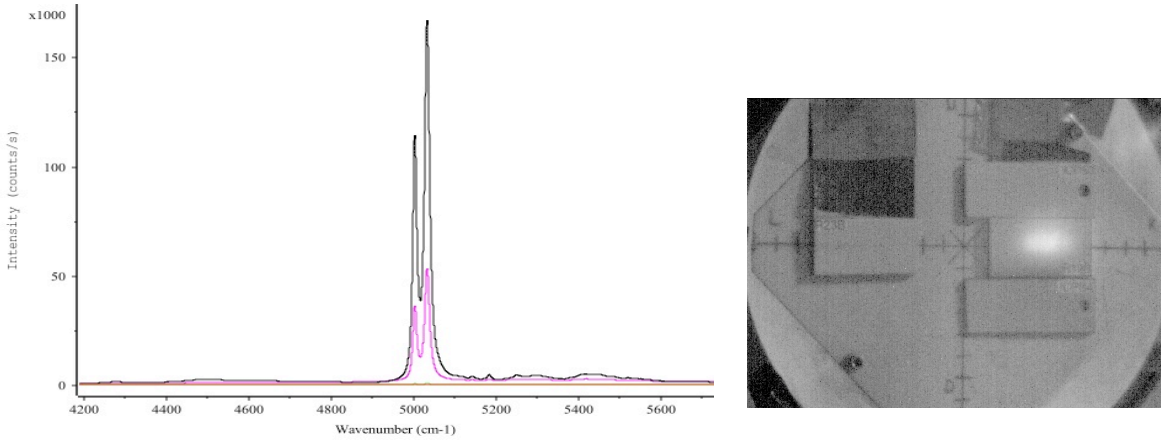

Fig. 2. R-lines at about 693 nm (left). Proton beam test (right)

In parallel with final process optimization, an automated flame spray system was designed and constructed. This final effort took about two months and culminated with the successful spraying of two new targets on the SNS site during June, 2009. The portable, automated spray booth is shown on the left of Fig. 3 and a completed target is shown on the right.

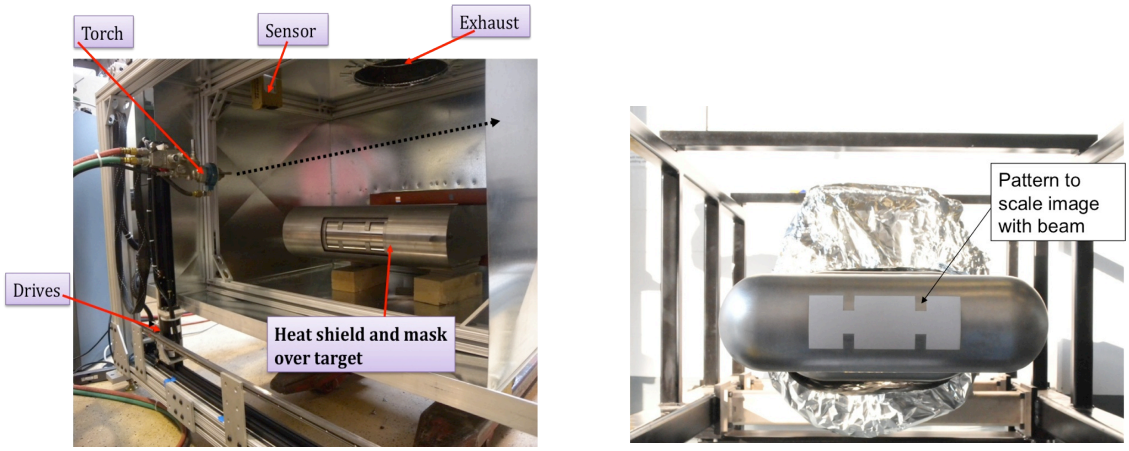

Fig. 3. Thermal spray equipment (left), coated target (right).

2.3. Optics

The primary optical components are shown in Fig. 4. On the proton beam window assembly, a diamond-turned aspheric convex mirror allows the entire width of the target to be viewed through a 25 mm diameter, 1 meter long aperture in the shield plug. At the top of this shield plug, a fused silica window isolates the target's helium environment from

atmosphere. At this location, a turning mirror combined with a radiation-tolerant triplet lens focuses the image onto the 1 mm diameter face of the imaging fiber. Finally, the 10,000 pixel, 11 meter long fiber carries the image out of the shield enclosure.

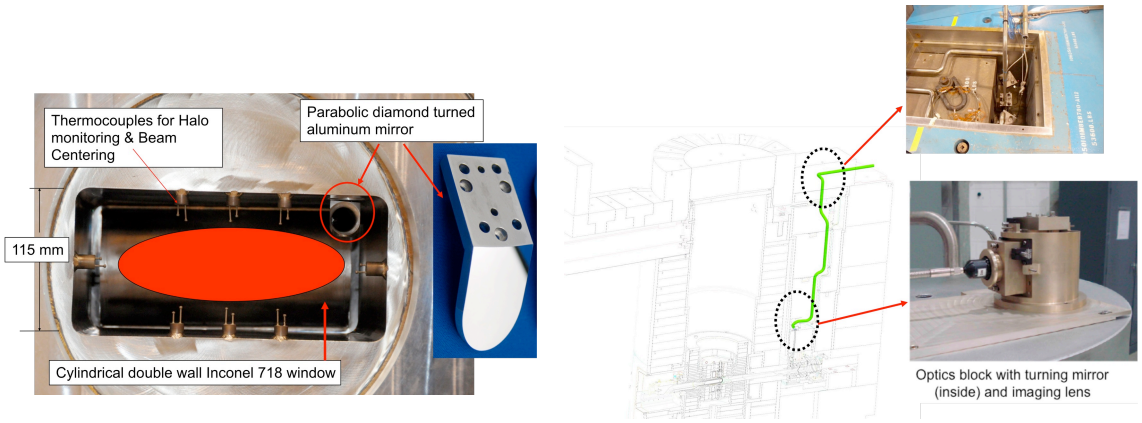

Fig. 4. The primary optical components: diamond turned convex mirror (left), triplet lens (lower right), and imaging fiber exiting the top of the shielding (upper right).

2.4. Image Acquisition

Because the optical system transports the image to a radiologically benign location, nearly any camera can be utilized without regard to radiation tolerance. A standard industrial camera with a CMOS sensor provided adequate signal to noise for initial operations, but as the coating degrades and light output decreases, a lower noise camera will be considered. The camera interface complies with the GigE Vision standard. Image acquisition and on-line analysis is performed in LabVIEW on a Windows PC platform. To integrate with the EPICS-based control system, EPICS IOC software runs on the same PC. It communicates with LabVIEW via shared memory, and with the control room via Channel Access over Ethernet. A custom PCI card receives timing events from the global event link and data from the real-time data link. This card produces the external trigger for the camera. To maintain signal integrity, all timing and data communication signals are carried in optical fiber.

3. Operation with Beam

3.1. First Images

After the Summer 2009 shutdown, the SNS accelerators were started up again in early September, 2009, and beam was transported to the target, initially at repetition rates of 1 Hz or less. As shown on the left in Fig. 5, the new imaging system captured the very first pulse on the new target. The images are color-mapped to enhance contrast. With less than 10^{11} protons, this pulse was about 0.1% of nominal intensity and the resulting luminescence barely exceeds the readout noise of the CMOS camera. Increasing the single pulse intensity to an intensity of about $5*10^{13}$ protons resulted in the cleaner image on the right in Fig. 5. Here, the beam fills the nominal footprint of 200 mm horizontally and 70 mm vertically. This beam also shows a small vertical offset, later corrected with upstream dipole magnets.

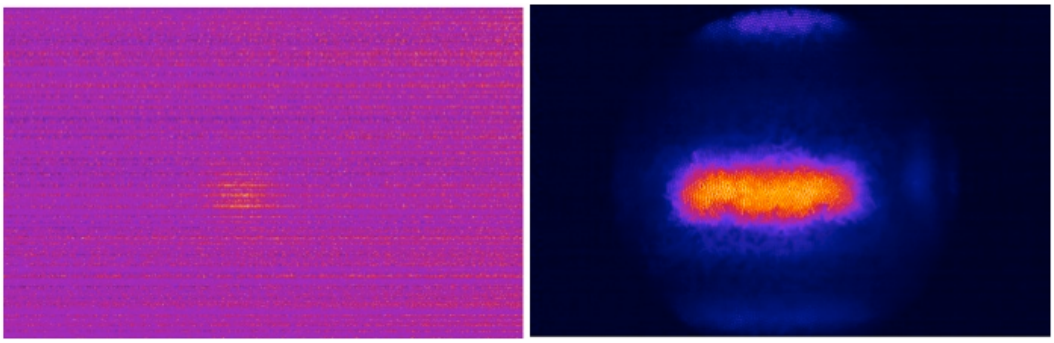

Fig. 5. Image of the first low intensity pulse (left). Image of a full intensity pulse (right).

3.2. Beam-based Calibration

Without a separate optical path for illumination, calibration is performed with the beam itself. Two calibration techniques are performed periodically to characterize the system: 1) geometric calibration to locate camera pixels in real-world units and 2) amplitude calibration to convert light intensity measured at each pixel into a proton density on target. For both techniques, data analysis is performed off line to produce a small number of calibration parameters that can be utilized by the on-line software.

Geometric calibration is performed by illuminating the edges of the coating pattern with an expanded proton beam. The previously measured dimensions of the coating pattern are used to calculate the geometric scale factors and offsets. Unfortunately, identification of the coating edges is hampered by lower than expected resolution and contrast. This is believed to be caused by chromatic aberration and will be addressed in the next system upgrade.

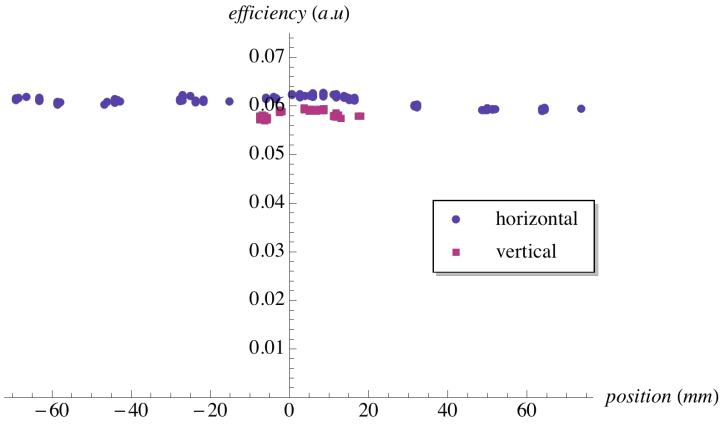

Fig. 6. Result of scanning a small beam across the target coating.

The amplitude calibration technique utilizes a beam of small transverse extent (about 15 by 25 mm RMS). While scanning the beam across the target face, images are recorded along with the single bunch charge as measured by an upstream current transformer. At each location, the central portion of the beam is fitted with a two dimensional Gaussian and the peak value is normalized with the bunch charge. The results shown in Fig. 6 show reasonable uniformity across the central region of the coating area. Using a small beam centered on the target, an amplitude scale factor (to convert pixel amplitude into proton

density) is determined by assuming that 96% of the proton beam lands on the coating. The other 4% is assumed to be lost via large angle nuclear scattering during passage through the upstream proton beam window.

3.3. Gas Scintillation

Over the first 100 MW-hours of beam energy on the coated target the light output dropped significantly. The camera integration time was progressively increased to compensate for this decreased output and eventually a glow appeared in the lower right section of the image (see the image on the left in Fig. 7). This glow is probably due to scintillation of the Helium gas upstream of the target and its intensity is consistent with previous estimates [2]. Looking downstream, the optical system views the target from the upper left, and therefore light from the incoming beam appears on the lower right portion of the image.

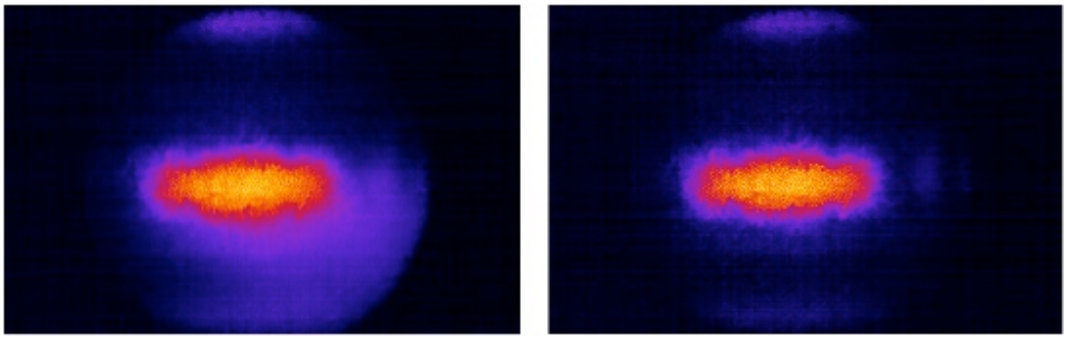

Fig. 7. Image during beam passage (left), image after beam passage (right).

By delaying the camera shutter, light from the short-lived gas scintillation can be rejected and the image is then dominated by the longer lifetime emission from the target coating. The right side of Fig. 7 demonstrates the effect of delaying the shutter opening time until 4 microseconds after beam passage. Since this should offer a more accurate representation of the proton density, the standard operation now includes this delay.

3.4. Coating Lifetime

As noted in the previous section, light output decreased during early operation. Fig. 8 shows the light output plotted against integrated beam power on target for two regions of the image. The points labeled “beam region” represent light from the central area of the image and should be dominated by light from the target surface. The points labeled “gas region” represent light from the lower right area of the image and should be dominated by light from the upstream gas. At 100 MW-hrs, the alumina-based coating had suffered about 0.1 DPA of damage, primarily from neutron irradiation. The rapid luminescent reduction prior to this is believed to be the result of F-center formation that results in decay channels that compete with photon emission at the R-lines. This effect is known to saturate near 0.1 DPA and the plot shows evidence of this.

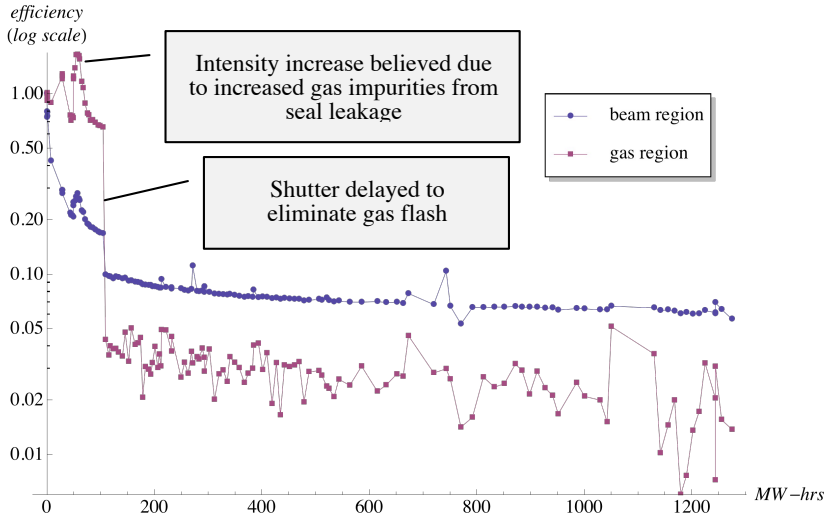

Fig. 8. Light output for two different regions of the image, plotted versus integrated beam power on target and normalized to initial value.

3.5. Spectral Measurements

After several hundred MW-hours of beam on target, the camera was temporarily replaced with a spectrometer and the spectrum shown in Fig. 9 was observed. The expected R-lines are visible at 693 nm, but they are joined by lines indicating emission from Hydrogen, Oxygen, Helium, and others. Just below 400 nm, a weak line at the emission wavelength of an F-center in alumina is barely apparent. Further measurements and analyses are planned.

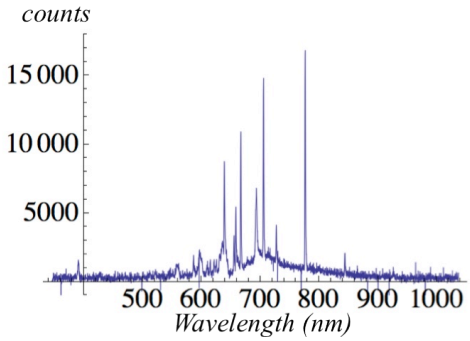

Fig. 9. Beam-induced spectrum observed after several hundred MW-hours on target.

3.6. Operational Examples

The imaging system has already proven itself as a sensitive monitor of relative proton density. When issues with upstream instrumentation led to the beam density being inadvertently tuned to a value that was higher than desired (on 10/22/09), the situation was immediately revealed by the imaging system. The plot in Fig. 10 (left side) shows the horizontal projection of the beam intensity, revealing the change in the beam profile.

Absolute accuracy of beam density measurements is still not proven and the right side plot in Fig. 10 depicts an unwelcome trend. Predicted and measured profiles seem to diverge over time. Understanding this discrepancy is the focus of current R&D efforts.

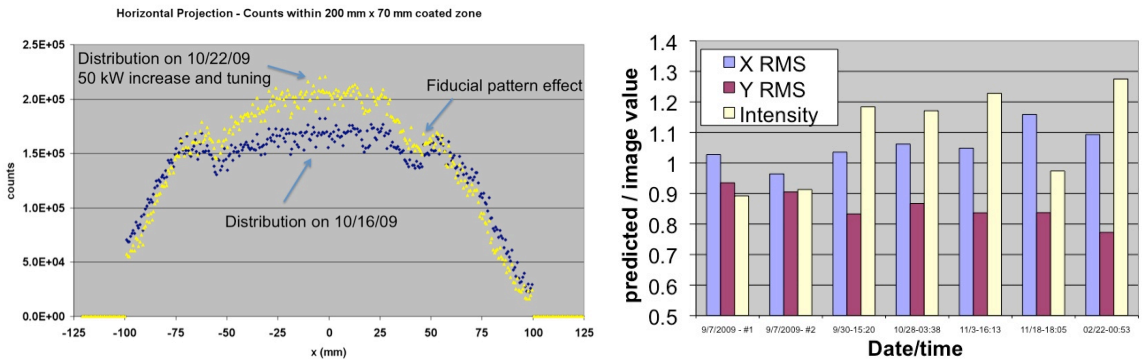

Fig. 10. Two different profiles (left), and comparison of predicted and measured beam properties (right).

4. Outlook and Plans

By mid-2010, the target will be due for another replacement. In preparation, the automated coating system will receive motion control upgrades, and the coating process will be more completely characterized. Although the Chromium doped alumina will still be used, enhancements to the feedstock powder and the processing conditions will be evaluated to ensure not only required luminescence but also improved robustness. By the end of 2010, the proton beam window will probably be replaced, providing an opportunity to upgrade the optics. The following enhancements are under underway: addition of a diffractive optical element to correct chromatic aberration, increased magnification, and an increase in imaging fiber pixels from 10,000 to 20,000. A second optical path is also being added to facilitate additional optical configurations and illumination options.

In parallel with these developments, an R&D effort continues with the goal of understanding the behavior of the irradiated coating. Time-gated imaging spectroscopy will characterize the emission spectrum more completely. These observations will be compared to calculations of the coating's response to protons, neutrons, and gammas. Decay times from tens of microseconds to a few milliseconds have been observed, and correlation studies aimed at identifying the underlying phenomena are underway. Reactor-based irradiation of samples may be used to rapidly measure radiation effects. Finally, design studies are proceeding on other applications, including an imaging system for the SNS Ring Injection Dump.

5. Acknowledgements

Many people contributed to this effort over the past years including: S. Baader, J. Colmenares, D. Feldman, R. Fiorito, C. Jensen, E. Kenik, S. McTeer, S. Murray, T. Pennisi, M. Plum, Shkvarunets, K. Thomsen, W. Wagner, and R. White.

6. References

[1] B. Riemer, these proceedings (2010).

[2] T. J. McManamy, et. al., "SNS Target Beam Profile Viewscreen Design and Operation", *AccApp* (2007).

[3] T. J. Shea, et. al, "Status of Beam Imaging Developments for the SNS Target", *DIPAC 2009* (2009).